Journal of Physics D:
Applied Physics

PURPOSE-LED
PUBLISHING™

PAPER

Design and optimization of millimeter-scale electroadhesive grippers

To cite this article: Jared D West *et al* 2020 *J. Phys. D: Appl. Phys.* **53** 435302

View the article online for updates and enhancements.

You may also like

- Force evaluation of electrostatic gripper with arrayed fibers consisting of parallel and coaxial electrodes
Shigeki Saito, Kazuteru Kawamura, Radon Dhelika et al.
- Optimization and experimental verification of coplanar interdigital electroadhesives
J Guo, T Bamber, M Chamberlain et al.
- A comparison of critical shear force in low-voltage, all-polymer electroadhesives to a basic friction model
Abraham Simpson Chen and Sarah Bergbreiter

This content was downloaded from IP address 71.249.71.149 on 31/10/2026 at 02:58

IOP Publishing Journal of Physics D: Applied Physics

J. Phys. D: Appl. Phys. **53** (2020) 435302 (12pp) https://doi.org/10.1088/1361-6463/aba1b0

Design and optimization of millimeter-scale electroadhesive grippers

Jared D West[1,2], **Joni Mici**[2], **Jeffrey F Jaquith**[2,3] **and Hod Lipson**[2]

[1] Department of Physics, Columbia University, New York, NY 10027, United States of America
[2] Department of Mechanical Engineering, Columbia University, New York, NY 10027, United States of America
[3] Department of Electrical Engineering, Columbia University, New York, NY 10027, United States of America

E-mail: jdw2194@columbia.edu

Received 1 May 2020, revised 24 June 2020
Accepted for publication 1 July 2020
Published 31 July 2020

Abstract

Electroadhesion is a complex physical phenomenon often used for astrictive prehension of a wide range of materials. Particularly effective at grasping millimeter-scale objects, electroadhesion is increasingly relevant to robotics, automation, and electronics manufacturing. This work presents a generalized optimization strategy and experimental validation of two-dimensional electroadhesors for gripping of millimeter-scale objects utilizing sub-millimeter-scale design parameters. Numerical electroadhesor optimization was based on three-dimensional electrostatic field simulations in COMSOL Multiphysics while experimental validation was performed through the gripping of incrementally increasing weights. Simulations and experiments were designed for the electroadhesion of objects with 1.6 mm thickness and using an applied voltage differential of 600 V. The spacings between electroadhesor pads and the width of the pads were varied to determine optimal parameters. To generalize results as much as possible, optimal values for each parameter are expressed as a ratio of pad area to the bounding box area of the electroadhesive element; the optimal electroadhesor pad spacing has been shown to be 0.5 mm and the optimal ratio has been shown to be 0.75 for both conductive and insulating objects of 1.6 mm thickness. Having determined the optimal design parameters, we present a step-by-step design methodology for electroadhesive elements intended to grasp both conductive and insulating millimeter-scale objects.

Keywords: microgrippers, electroadhesion, electrostatic gripper, layered assembly

(Some figures may appear in colour only in the online journal)

1. Introduction

1.1. Electroadhesion

Electroadhesion is the attractive force which occurs between two objects when there is a voltage differential between them [1, 2]. Electroadhesion is a complex phenomenon, influenced by over 33 independent factors [3]. As a type of astrictive prehension [4], electroadhesion has been incorporated into a variety of gripping mechanisms, including textile gripping [5], robotic end-effectors [1, 2], climbing robots [1, 6], modular robots, additive manufacturing [7], astronautical applications [8, 9], and selective pick-and-place technologies [2, 7, 10]. In the simplest form, electroadhesors consist of two conductive pads capable of holding a voltage differential between them. Adding a dielectric material between the pads enables grasping of conductive objects as shown in figure 1(A). A positive voltage is established on one pad, while a negative voltage or a path to ground is established on the other. This voltage differential generates an electric field that emanates from the gap between the two pads into the object material. The electric field

© 2020 IOP Publishing Ltd Printed in the UK
All rights, including for text and data mining, AI training, and similar technologies, are reserved.

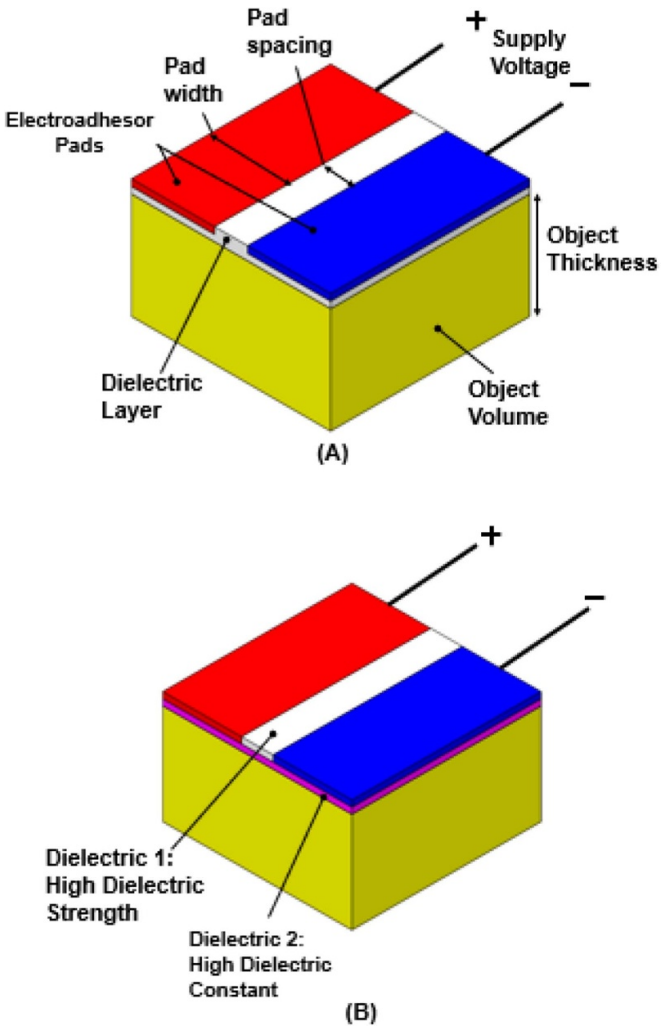


Figure 1. (A) Anatomy of a simple electroadhesor equipped with a dielectric shield to enable gripping of conductive objects. (B) Two-dielectric electroadhesor design.

is responsible for the electroadhesive force between the pads and the object. The geometry of a standard electroadhesor is shown in figure 1(A) [7]. Figure 1(A) serves as a visual reference to identify crucial electroadhesor design parameters: pad spacing, pad width, and object thickness. These parameters will be referenced repeatedly throughout this work.

1.2. Physical principles of electroadhesors

Having outlined the conceptual working principles of an electroadhesor, it is now appropriate to lay out the physical and mathematical basis behind those working principles. Depending on the material properties of the object, the primary physical mechanism for electroadhesion differs. For conductive objects, the primary mechanism of electroadhesion is a net force resulting from induced charges through the motion of free electrons; for insulative objects, the primary mechanism is a net force due to electrical polarization of molecules [11]. For both conductive and insulative objects, the following theoretical exercise will assume that perfect surface contact exists between the electroadhesor and the target object, meaning there is no air gap between the surfaces of the electroadhesor and the target object.

Electroadhesion of conductive objects due to electron migration involves two distinct electrical forces, the Coulomb force and the Johnsen–Rahbek force [12]. For the purpose of this paper, discussion will be limited to the Coulomb force, as the electroadhesors in consideration are of the Coulomb type [13] and thus the authors assume that the dominant force is the Coulomb force and the Johnsen–Rahbek force can be ignored. Assuming the object is a perfect conductor, the Coulomb force can be modeled as follows:

$$F_{Coulomb} = q_{induced}E \tag{1}$$

where $q_{induced}$ is the total charge induced on the surface of the conductor and E is the electric field generated by the electrodhesor. The induced charge can also be expressed as a function of the electric field generated by the electroadhesor. This is concisely expressed in terms of the induced surface charge σ [14]:

$$\sigma = \varepsilon_0 E \tag{2}$$

$$q_{induced} = \sigma A_{surface} = \varepsilon_0 E A_{surface} \tag{3}$$

where E is again the electric field generated by the electroadhesor and $A_{surface}$ is the surface area of the object in contact with the electroadhesor. Finally, equation (3) can be substituted into equation (1) to yield equation (4):

$$F_{Coulomb} = \varepsilon_0 E^2 A_{surface}. \tag{4}$$

The primary takeaway from this equation is that the electroadhesive force is proportional to the square of the electric field generated by the electroadhesor, which means that maximizing the field output of the electroadhesor will result in optimal gripping force.

Assuming insulators behave as linear dielectrics, the electroadhesion of insulators due to polarization can be expressed by the linear polarization equation [11]:

$$P = (\varepsilon - 1)E \tag{5}$$

where ε is the dielectric constant of the object. The electroadhesive force due to polarization can then be computed as follows:

$$F = PEA_{surface} \tag{6}$$

$$F = (\varepsilon - 1)E^2 A_{surface}. \tag{7}$$

Again, we find that the electroadhesive force is proportional to the square of the electric field generated by the electroadhesor. Both equations for electroadhesive force in conductors and insulators dictate that maximizing electric field generated by the electroadhesor will result in maximum electroadhesive gripping force. Such an electric field optimization strategy has been used in previous research and has proven effective in both

simulation and experiment [11, 12, 15]. These equations, however, are only a simple theoretical model and cannot be used to accurately predict the force generated by electroadhesion due to the complex nature of the phenomenon.

1.3. Optimization of millimeter-scale electroadhesors

Work by Guo *et al* has been successful in optimization of electroadhesor geometry for pad spacing of 1 mm and greater [12, 16], but has not explored sub-millimeter pad spacings. Ruffatto *et al* tested electroadhesors with pad spacings down to 0.6 mm and conclude that the smaller the pad spacing, the greater the generated electric field and thus the greater the electroadhesive force [17]. This work neglects to account for the fact that the electric field emanating from a small pad spacing quickly decays as it extends into the object volume [17], meaning only a small portion of the object material near its surface will contribute to the electroadhesive force [12]. Thus, while previous research has sought to optimize electroadhesor geometry, a research gap remains in optimization of electroadhesors with sub-millimeter-scale features intended to grip millimeter-scale objects. Electroadhesion has been theorized to be a particularly practical gripping method on small scales [18], further motivating the optimization of electroadhesors on this scale.

This paper addresses the research gap in design paradigms of sub-millimeter-scale electroadhesors for gripping millimeter-scale objects. We build upon previous work in electroadhesor optimization by determining optimal sub-millimeter electroadhesor parameters for the gripping of millimeter-scale objects. The lower bound of the sub-millimeter parameter space is dictated by practical manufacturing limits. Precision electronics manufacturers are limited to circuit trace and spacing of 0.1254 mm [19]. Moreover, as objects approach the micro- and nano-scales, van Der Waals forces begin to dominate the underlying physics [10, 20]. The scope of this paper, therefore, is the sub-millimeter parameter space between 0.1 mm and 1.0 mm.

Optimal parameters were found through a systematic set of 3D electrostatics simulations in COMSOL Multiphysics with the goal of maximizing the average electric field magnitude over the object volume. The electric field magnitude is defined as the square root of the sum of the squares of the x, y, and z-components of the field, or $(E_x^2 + E_y^2 + E_z^2)^{1/2}$. Experimental verification was subsequently performed with a set of five different electroadhesor designs from the simulation set. After determining optimal design parameters in this space, a novel design process for electroadhesor geometry with sub-millimeter-scale parameters can be determined.

2. Simulation

2.1. Simulation setup

The electroadhesor geometry consists of alternating high and low voltage pads 10 mm in length patterned over a 10 mm horizontal distance. The object lies below the pads with a dielectric layer in between. Perfect surface contact was assumed between the electroadhesor and the object and therefore there was no air gap added to the simulation. Although this geometry can be simplified to a 2D model [12], COMSOL 3D simulation was utilized so that electroadhesors of arbitrarily complex geometry could be tested in the same manner as this simple electroadhesor model. The geometry of the simulated electroadhesor was set with non-variable pad, dielectric, and object thicknesses. The pad and dielectric thicknesses were set at 0.1 mm and 0.08 mm respectively based on dimensions of real electroadhesors manufactured by the authors in previous research [7]. It has been shown that the pad thickness has a negligible effect on electroadhesor performance and that the dielectric thickness should be as small as possible to achieve maximal attractive forces [12]. The object thickness was set at 1.6 mm motivated by potential use cases of electroadhesors on this scale, such as electronic component pick and place and layered assembly [7]. All layers of geometry in the simulation were meshed using tetrahedral elements of maximum size 0.55 mm and minimum size 0.04 mm automatically populated by COMSOL's mesh seed algorithm. A 2D cross-section of the simulation geometry is presented in figure 2.

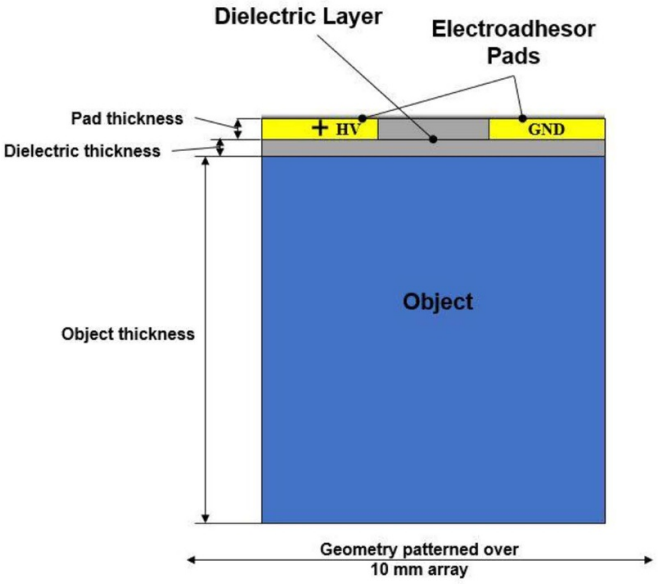


Figure 2. A 2D cross-sectional schematic of the simulation geometry which displays all non-variable simulation geometry parameters. The actual simulation geometry is 3D, extending 10 mm into the plane of the page.

The remaining design parameters, pad width and pad spacing, were varied to determine the values which produce the maximal average electric field magnitude over the object volume in both conductive and insulative objects. The ratio of the pad spacing to the pad width will also be considered as an additional parameter for optimization. It is important to acknowledge that the simulation geometry is a simplified model that ignores pad edge effects present in a typical interdigitated electroadhesor. However, the pad width and pad spacing parameters in the simulation geometry are basic features of any electroadhesor and are directly transferable to more complex geometries. Furthermore, the ratio of pad spacing to

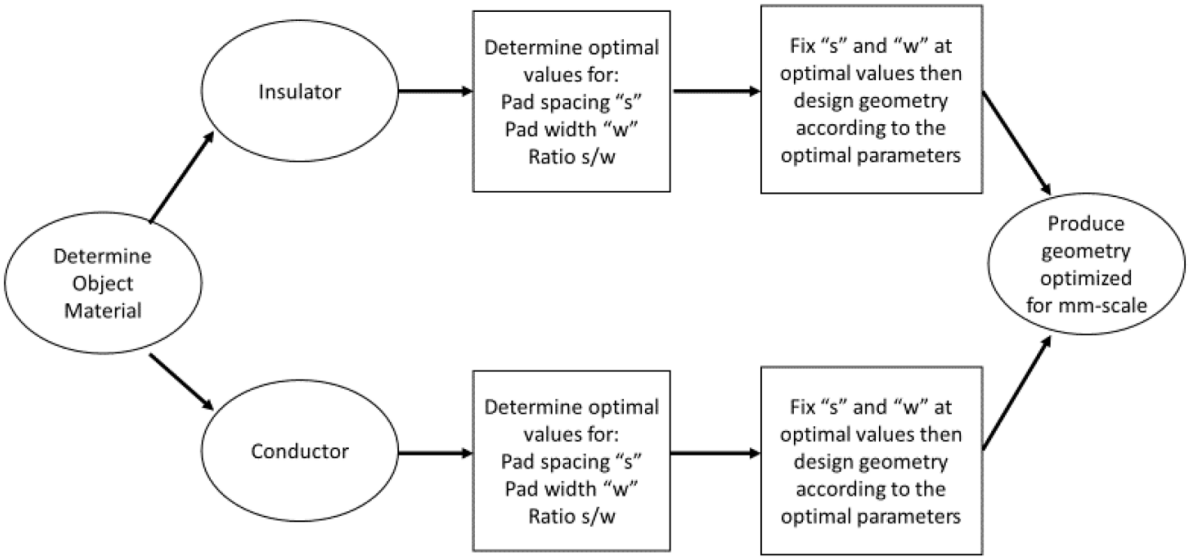


Figure 3. Electroadhesor optimization logic tree.

pad width can be generalized to incorporate the pad edges of an arbitrary electroadhesor design such that the optimized parameters from simulation are applicable to any interdigitated geometry at this scale; this is done by expressing the ratio of the pad area to the area of the bounding box in which the electroadhesor lies. The pad area is defined as the pad width multiplied first by its length and then by the number of pads in the electroadhesor. The bounding box area is defined as the area enclosed by the outer perimeter of the electroadhesor. Optimizing the ratio of the pad area to the bounding box area will allow for the optimization to be generalized to electroadhesors of any bounding box size with intent to grip millimeter-scale objects. The above logic is concisely presented in figure 3.

Table 1. Geometric, material, and physical parameters for the simulation set.

Non-variable simulation parameters	
Dielectric layer dielectric constant	3.4
Insulative substrate dielectric constant	4.0
Aluminum conductivity	5.998×10^7 S m^{-1}
Copper conductivity	3.774×10^7 S m^{-1}
HV terminal voltage	600 V
GND terminal voltage	0 V
Dielectric layer thickness	0.08 mm
Pad thickness	0.10 mm
Object thickness	1.60 mm

2.2. Material selection

Following electroadhesor design, electroadhesor geometry was imported to COMSOL Multiphysics 5.4 to implement simulations. Materials were assigned in COMSOL by defining dielectric constants and conductivities for the various materials which comprise the electroadhesor. The pads were assigned material properties of copper, most notably an electrical conductivity of 5.998×10^7 S m^{-1}. The dielectric was given a dielectric constant of 3.4 to simulate common dielectrics used in circuitry such as soldermask. Since electric field magnitude averages will differ between conductive and insulative objects, these two cases will be individually simulated and optimized. The object was either modeled as an insulator with dielectric constant 4.0 or as a conductor with the material properties of aluminum. Non-variable simulation parameters are collected in table 1.

Additionally, a novel design of a two-dielectric electroadhesor was also explored in simulation as shown in figure 1(B). The dielectric material in an electroadhesor serves two distinct purposes: to prevent a short circuit between electroadhesor pads and to prevent a short circuit into the object material. The two-dielectric electroadhesor design incorporates two different dielectric materials into the electroadhesor to fulfill these distinct purposes separately. The first dielectric material is situated between the electroadhesor pads and is chosen to have a high breakdown voltage such that the voltage between pads can be maximized without danger of dielectric breakdown. The second dielectric material is situated between the electroadhesor pads and the object material and is chosen to have a high dielectric constant to promote the propogation of the electric field to the object volume. The two-dielectric design is depicted in figure 1(B) with dielectric 1 depicted in white and dielectric 2 in pink. Since the dielectric strength and dielectric constant of a material are not directly related, the two dielectric approach allows for an optimal material for each individual function of the dielectric in the electroadhesor and will consequently enhance electroadhesor performance.

Teflon was selected for dielectric 1 for its high dielectric strength (70 MV m^{-1}). Neoprene was selected for dielectric 2 for its dielectric constant of 6.7, nearly double that of soldermask and other similar dielectrics. The two-dielectric design was modelled in COMSOL by defining dielectric constants of 2.1 and 6.7 for Teflon and neoprene, respectively. The

Table 2. Material and physical parameters for the two-dielectric simulation.

Two-dielectric simulation parameters	Single dielectric design	Two-dielectric design
Single dielectric constant	3.4	N/A
Dielectric 1 dielectric constant	N/A	2.1
Dielectric 2 dielectric constant	N/A	6.7
Breakdown voltage	39 kV	70 kV
HV terminal voltage	34 kV	65 kV
GND terminal voltage	0 V	0 V

two-dielectric model was compared against a single dielectric model with a dielectric constant of 3.4 and a dielectric strength of 39 MV m^{-1} which again corresponds to solder-mask material. The geometry of the electroadhesor in both the single dielectric and two-dielectric simulations is identical with a spacing of 1.0 mm and a spacing/pad-width ratio of 1.0. The dielectric strength was incorporated into each model by applying different voltages in the single dielectric and two-dielectric simulations; the voltage was set to be 5 kV below the breakdown voltage for the electroadhesor in each of the two simulations. The breakdown voltage is calculated simply by multiplying the dielectric strength of the dielectric material between the pads by the pad spacing. For the two-dielectric model, the breakdown voltage is 70 kV and thus the voltage differential was set at 65 kV; for the single dielectric model, the breakdown voltage is 39 kV and thus the voltage differential was set at 34 kV. It is important to acknowledge here that the two-dielectric simulation is operating at nearly twice the voltage at which the single dielectric simulation operates. This is only possible due to the material properties of dielectric 1 in the two-dielectric design, as the high dielectric strength allows for an increased operating voltage compared to the single dielectric design; if the single dielectric design were operated at the same voltage as the two-dielectric design in this case, breakdown voltage would be exceeded, and the single dielectric electroadhesor would be ineffective. Simulation parameters for the two-dielectric simulation are collected in table 2.

2.3. Simulation methods

Electroadhesors were simulated in COMSOL to determine average electric field magnitude in the object volume. Simulations were carried out using the COMSOL electrostatics module. Voltages of 600 V and 0 V (ground) were applied to electroadhesor pads to establish a 600 V potential difference between pads. This operating voltage was chosen as it is under the breakdown voltage threshhold for the sub-millimeter pad spacing regime under consideration. The pad spacing was varied 0.1 mm in each simulation, beginning at a minimum value of 0.1 mm up to a maximum value of 1.2 mm. In this stage of the simulation, the pad spacing to pad width ratio was maintained at a constant value of 1.0. This process was first conducted with an insulative object and was then repeated with a conductive object. Following each simulation run, the average electric field magnitude in the object volume was recorded. The average electric field magnitude was calculated using COMSOL's volume average function, which performs a numerical integration of the electric field magnitude across all nodes in the object volume and subsequently divides this integral by the volume of the object.

Simulation was used to first determine optimal spacings and then continued with a variation of the pad width for the optimal spacings, thus varying the pad spacing to pad width ratio. The pad width was varied in each simulation such that the ratio of pad spacing to pad width changed by a value of 0.1, beginning at a ratio of 0.2 and increasing to 1.0. The results of this stage of simulation produced the final, optimized sub-millimeter pad spacing and pad width parameters.

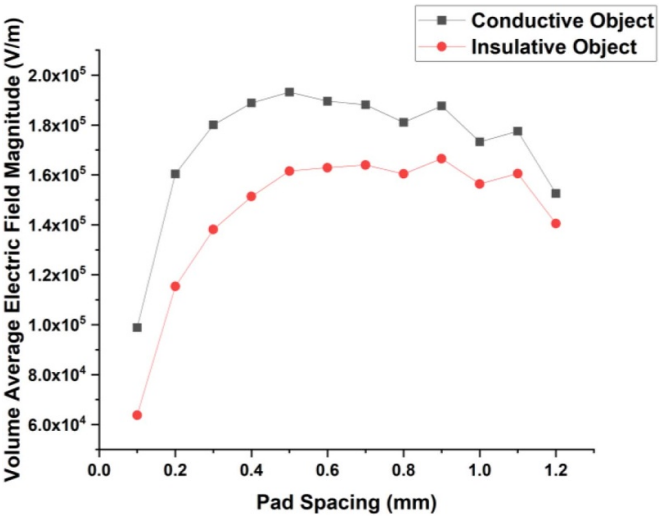


Figure 4. Volume average electric field magnitude for insulative and conductive objects. The maximum average field magnitude for insulative objects occurs at a spacing of 0.9 mm; for conductive objects the maximum occurs at a spacing of 0.5 mm.

3. Simulation results

3.1. Optimal pad spacing

The maximum volume electric field magnitude was 1.67×10^5 V m^{-1} for the insulative object and was generated by the 0.9 mm spacing as shown in figure 4. Though the 0.9 mm spacing generated the maximum average field magnitude in the simulation set, the 0.5 mm, 0.6 mm, 0.7 mm, and 0.8 mm spacings all came within 3.68% of this maximum. The range of 0.5 mm to 0.9 mm spacings will be considered the optimal spacings for electroadhesion of an insulative object.

For a conductive object, the pad spacing which produced the maximal average electric field magnitude of 1.93×10^5 V

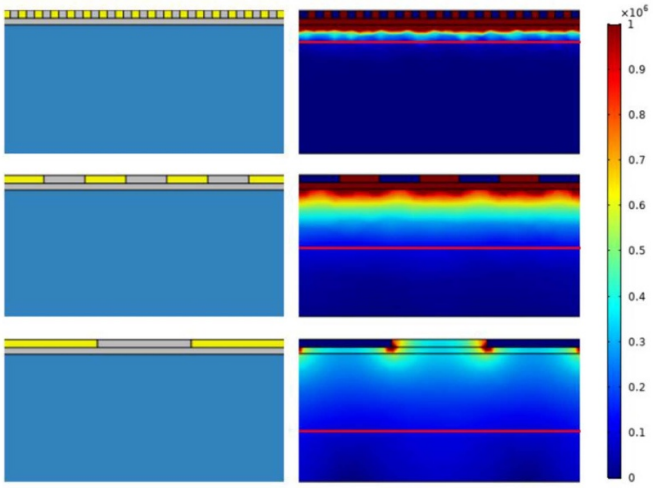


Figure 5. Visual representation of electric field magnitude in the object space for 0.1 mm spacing (top), 0.5 mm spacing (middle), and 1.2 mm spacing (bottom). Warm colors are regions of high field magnitude, while cool colors are regions of low field magnitude. As pad spacing increases, the depth plane moves further into the object space. The opposite is true for decreasing pad spacing. The optimal spacing of 0.5 mm situates the depth plane near the centre of the object space and produces the maximal volume average electric field magnitude in the object space.

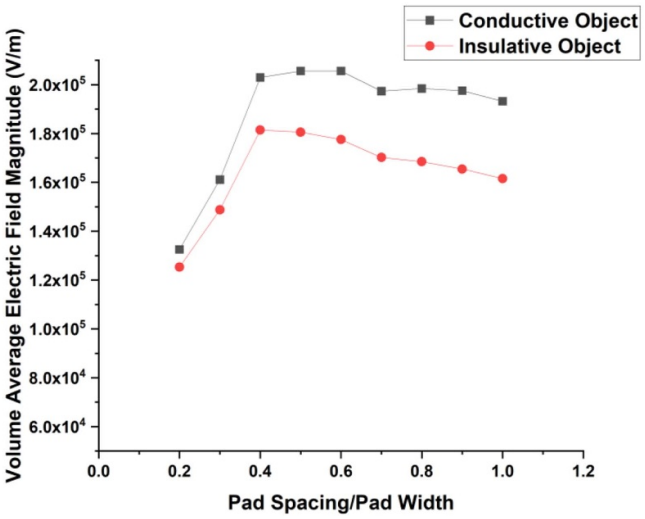


Figure 6. Volume average electric field magnitude as a function of the pad spacing to pad width ratio for insulative and conductive objects. The maximum average field for an insulative object occurs at a ratio of 0.4; the maximum for a conductive object occurs at a ratio of 0.5.

m^{-1} in the object volume was the 0.5 mm spacing. A distribution of the volume average electric field magnitude as a function of pad spacing can be seen in figure 4.

Figure 4 makes evident that the volume average electric field magnitude in the object space decays when the spacing grows larger than the optimal values and when the spacing shrinks smaller than the optimal values. Qualitatively, this can be understood by considering figure 5. Since the applied voltage is fixed at 600 V, the electric field magnitude between pads increases with decreasing pad spacing according to E = V/spacing. As spacings become smaller than the optimal range, the magnitude of the electric field near the pads is large but the field magnitude decays quickly as it extends into the object space. Conversely, as spacings become larger than the optimal range, the magnitude of the electric field near the pads is diminished, but the field magnitude decays less quickly as it extends into the object space. To further describe this qualitative behavior, the authors introduce the concept of the depth plane in figure 5, a two-dimensional plane through the object volume on which the surface average electric field magnitude is equal to the volume average electric field magnitude in the object space. as pad spacing increases, the depth plane moves deeper into the object thickness. A depth plane that is too shallow or too deep in the object space will result in a low average electric field magnitude over the object volume, while a depth plane near the center of the object volume produces the maximal average electric field magnitude over the object volume. The optimal pad spacings, then, generate electric fields which have a high magnitude, and which permeate sufficiently into the object space resulting in a depth plane near the center of the object thickness.

3.2. *Optimal pad spacing to pad width ratio*

Having determined optimal pad spacings for both conductive and insulative objects, the optimal pad spacing to pad width ratio could be determined. In order to reduce the number of geometrically unique simulations, the experimenters chose a single pad spacing value for both insulative and conductive objects. This meant that the geometry in the insulative and conductive object simulations was identical and only the material properties of the object were adjusted. A spacing of 0.5 mm was chosen because this spacing produced the maximum volume average electric field magnitude for the conductive object and a volume average electric field magnitude within a 3.0% margin of the maximum for the insulative object. The 0.5 mm spacing is also within the range defined as optimal for the insulative object.

For insulative objects, the pad spacing/pad width ratio that produced the maximum average electric field magnitude of 1.81×10^5 V m^{-1} in the object volume was 0.4, as can be seen in figure 6.

For conductive objects, the pad spacing/pad width ratio that produced the maximum average electric field magnitude of 2.06×10^5 V m^{-1} in the object volume was 0.5, as seen in figure 6.

3.3. *Two-dielectric design*

Compared to the standard single dielectric electroadhesor geometry, the two-dielectric design more than doubled the average electric field in the object volume. The standard design generated a volume average electric field magnitude of 9.82×10^6 V m^{-1}, while the two-dielectric design generated a volume average field magnitude of 1.90×10^7 V m^{-1}. This dramatic difference is demonstrated in the COMSOL graphics in figure 7.

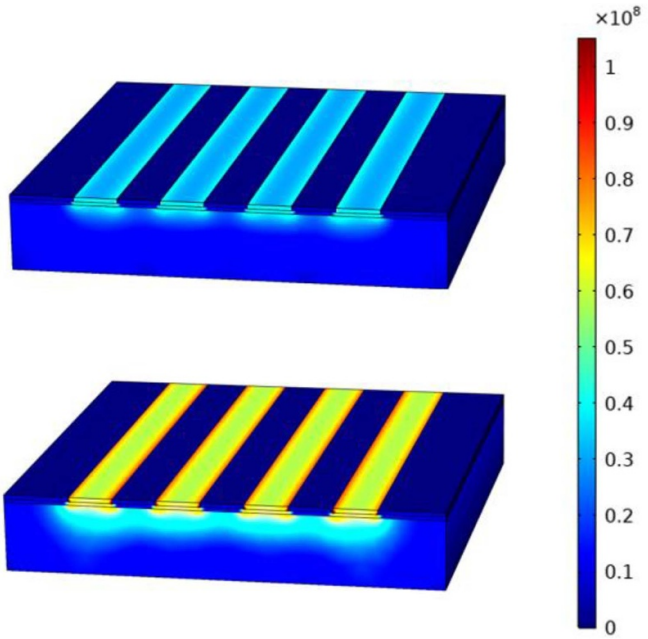


Figure 7. Visual representation of electric field magnitudes. The upper image is the single dielectric design while the lower image is the two-dielectric design.

4. Experimental validation

4.1. Electroadhesor design selection

Simulation results were validated through experimental testing of five electroadhesor geometries, shown in figure 8, which were designed based on the simulation results of sections 3.1 and 3.2. The selected geometries span three different spacings and three different pad spacing to pad width ratios in order to generate experimental data that relates to both the spacing optimization and the pad spacing to pad width ratio optimization simulations. Spacing is denoted by s and pad spacing to pad width ratio is denoted r. Selected electroadhesor geometries are numbered in descending order according to expected force generation from simulation results (1 generating greatest force, 5 generating least force); the expected force corresponds to the volume average electric field magnitude in simulation:

Electroadhesor geometries were designed as 3D models in SolidWorks 2019. The electroadhesors were bounded to a 42 mm by 42 mm square which was populated with a comb pattern governed by the aforementioned parameters, s and r. Pad widths on either side of the bounding box were fixed at 3 mm to facilitate soldering and electrical connections. A dielectric layer was not used in the electroadhesor design. The reason for this decision was two-fold: first, target objects in the experiment were insulators and thus do not require a dielectric layer, and second, adding a dielectric layer can be a source of error due to lack of dielectric thickness control in manufacturing. In order to compare the experimental results directly with simulation, another set of five simulations was designed to test the exact geometry of the electroadhesors in the experiment. Results of these simulations are displayed in figure 9. The highest electric field magnitude average in the object space

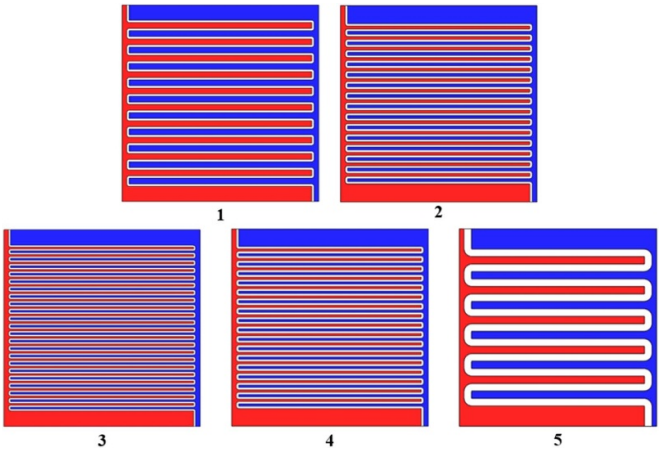


Figure 8. Electroadhesor designs used in experimental validation. (1) s = 0.5 mm, r = 0.4, (2) s = 0.5 mm, r = 0.8, (3) s = 0.4 mm, r = 1.0, (4) s = 0.5 mm, r = 1.0, (5) s = 1.6 mm, r = 1.0.

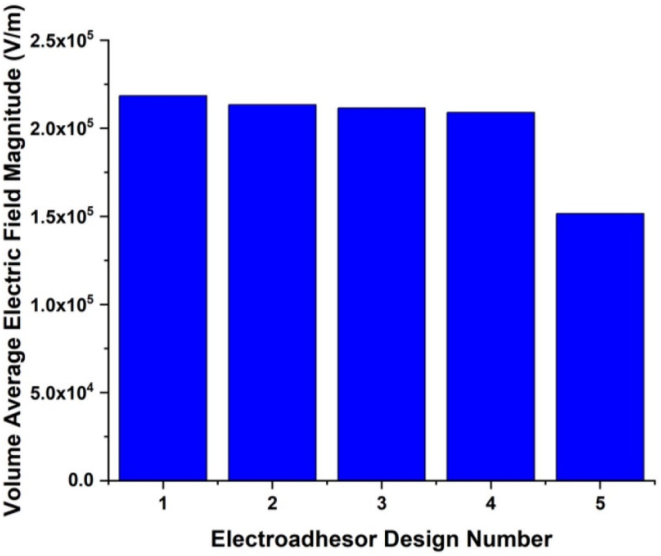


Figure 9. Volume average electric field magnitudes for simulations with geometry identical to experimental electroadhesors.

was still generated by the $s = 0.5$ mm, $r = 0.4$ electroadhesor design and therefore it was still expected to be the optimal design.

4.2. Manufacturing electroadhesors

After each electroadhesor was designed in SolidWorks, the geometry was exported as a STEP file and imported to Autodesk Fusion. Toolpaths for machining the electroadhesor from FR-4 PCB stock were then generated using Fusion's computer aided machining package. The FR-4 PCB stock has a 1.6 mm overall thickness with a 0.1 mm layer of copper on one side; this results in electroadhesor pads with a 0.1 mm thickness. Finally, toolpaths were exported from Fusion and passed to a CNC desktop mill (Othermill Pro) to execute the machining process.

Post processing for the machined electroadhesors involved simple cleaning and deburring. The electroadhesors were first vacuumed to remove any remaining waste material from the machining process. Steel wool was then used to scrub the electroadhesor surface, removing any copper burs around the edges of the electroadhesor pads; a razor blade was also passed over the electroadhesor surface to achieve the same end. Finally, the electroadhesors were cleaned with a soft sponge and water.

4.3. Testing setup

Electroadhesors were supplied high voltage by a DC transformer which was connected to a tuneable, voltage-limited power supply. Voltage output was measured with a Keysight 10076C High Voltage Probe. Electroadhesors were mounted to a computer-controlled XYZ gantry. The target object used in the experiments had a 1.6 mm thickness and was made of solid polylactic acid (PLA). PLA has a dielectric constant of 3.5 [21] which is comparable to the 4.0 dielectric constant used for the object in simulation. The PLA object shown in figure 10(A) was designed with features to hold two modular, 3D printed weights which could be exchanged to increase or decrease the object weight.

For each trial, a target object was placed on a platform which rests on the gantry's main platform. As seen in figure 10(B) the platform consists of a 3D printed plastic base which holds a compliant foam layer to allow compressibility, which maximizes surface contact between the electroadhesor and the object surfaces. The alignment jig snap fits to the corner of the object platform base; the jig simultaneously aligns the object on the platform and aligns the platform to the electroadhesor. To perform alignment, the object is first placed on the platform with its corner aligned to one of the jig's two alignment features. Then the electroadhesor is lowered to a height of 38.5 mm above the printer bed, and the jig's second alignment feature is manually fit to the corner of the electroadhesor.

Since the application of electroadhesors on this scale is to pick up small objects, the testing strategy was designed in a similar manner. The electroadhesor would be placed in contact with a PLA target object of a certain weight. The electroadhesor would then be pulled away from the object; if the object remained attached to the electroadhesor, the trial would be recorded as a successful pickup, and otherwise the trial would be considered a failed pickup. This process was repeated for each individual electrode from figure 11 with increasing object weights until the electroadhesor no longer performs successful pickups. The heaviest weight successfully picked up by a given electroadhesor would be considered its maximum weight, and from this, the authors can obtain the maximum force generated by the electroadhesor.

Conductive objects were not tested in this experiment due to the difficulty and cost of manufacturing weights using metals. However, considering the similarity in behaviour of conductive and insulative objects in both the theoretical models and simulation results, we argue that experimental validation performed with the insulative PLA object would also prove valid if tested with conductive objects.

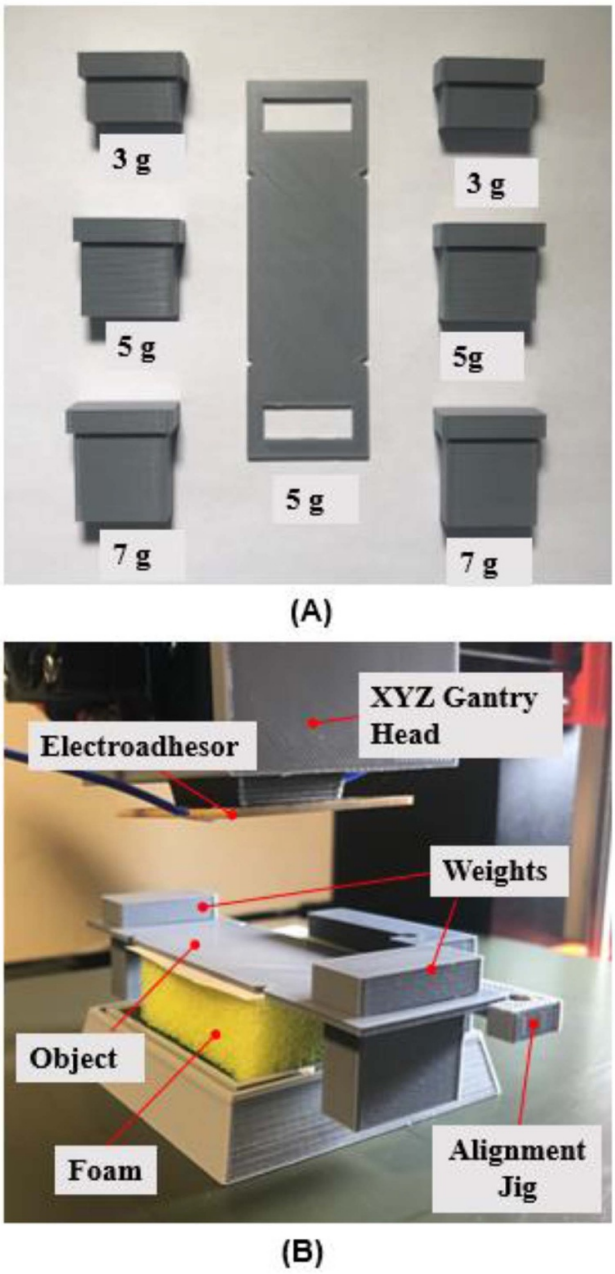


Figure 10. (A) Testing setup of XYZ gantry, electroadhesor, and weights and compliant foam. (B) PLA object with discrete weights.

4.4. Testing procedure

Each of the five electroadhesors was tested with discrete weights in increments of 2 g until the maximum weight was reached. The following sequence was executed for each trial:

1. Turn on power supply at 600 V.
2. Lower electroadhesor at a rate of 250 mm min^{-1}, placing it in contact with the target object, and compressing foam 0.25 mm
3. Pause 10 s.
4. Raise electroadhesor 8 mm above platform at a rate of 100 mm min^{-1}.

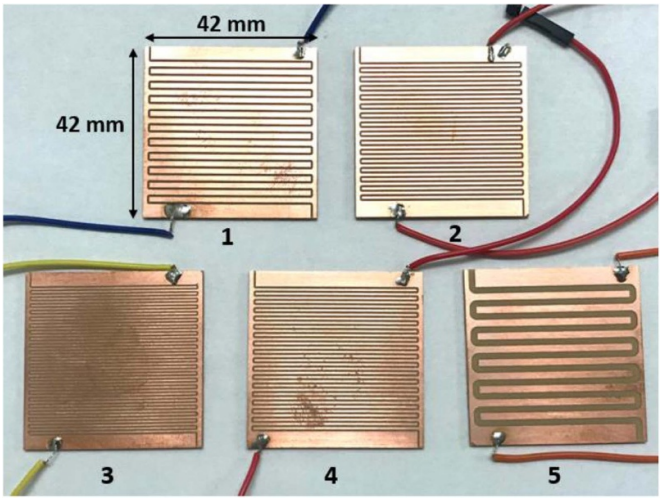


Figure 11. Manufactured electroadhesors corresponding to the five electroadhesor designs.

5. Record successful pickup if target object remains attached to electroadhesor; if object remains on platform or if object detaches from electroadhesor in step 4, record failed pickup.
6. Turn power supply off.

This sequence is shown visually in figure 12. Before increasing weight, the electroadhesor was required to complete three successful pickups over a maximum of five trials. If three failed pickups were recorded over the course of five trials, the weight was considered beyond the maximum weight of the electroadhesor.

4.5. Results

Electroadhesor geometry 1 generated the greatest force of all tested electroadhesors by far with a maximum successful pickup weight of 39.5 g, which is equivalent to a force of 0.3871 N. This experimental result is very well in line with the predicted result based on simulation. Similarly, the maximum forces generated by electroadhesor geometries 2–5 correspond very well to volume average electric field magnitude simulation results. It is important to recall the discussion in section 1.2, where the electroadhesive force was shown to be proportional to the square of the applied electric field in the object space. In figure 13 the maximum force generated in experiment is plotted as a function of the square of the electric field in the object space from simulation for each electroadhesor geometry. As predicted by the theoretical model, this figure shows a linear trend between the maximum force from experiment and the square of the average electric field magnitude in the object space from simulation with a Pearson correlation coefficient of 0.834. Considering electroadhesion is a complex phenomenon dependent on 33 independent factors, some deviation from the linear relationship between the square of the electric field and electroadhesive force developed in section 1.2 should be expected. Despite these factors, the 0.834 Pearson coefficient remains a strong linear trend that shows a strong correlation between simulated volume average electric field magnitude and experimental maximum force. This result validates and shows the effectiveness of our electroadhesor optimization technique, that is, the maximization of simulated volume average electric field magnitude in the object space through adjustment of pad spacing and pad spacing to pad width ratio parameters.

5. Discussion

5.1. Optimized geometry

This paper has addressed the aforementioned research gap with the successful design, simulation, and experimental verification of optimized electroadhesor geometry for millimeter-scale objects using sub-millimeter-scale design parameters. Previous work by Guo *et al* has theoretically and quantitatively optimized electroadhesor geometry with a minimum of 1 mm spacing, while work by Ruffatto *et al* optimized electroadhesor geometry with a spacing as small as 0.6 mm under the assumption that the smaller the spacing, the greater the electroadhesor performance [11, 12, 15, 16]. Our work has more fully explored the sub-millimeter parameter space, finding optimal sub-millimeter parameters through simulation, and verifying simulation results through a quantitative relationship between simulated volume average electric field magnitudes and experimentally measured maximum electroadhesive force. The optimized electroadhesor for both insulative and conductive objects with a 1.6 mm thickness was found to have a 0.5 mm pad spacing and a 0.4 pad spacing to pad width ratio. This optimization allows for the design of high-performance electroadhesors for target objects on the millimeter scale. Such an electroadhesor is highly applicable in modern manufacturing. Many common electronics components such as transistors and microchips are on the order of 1.6 mm thickness and must be quickly and accurately positioned to manufacture complex electronic devices. Furthermore, operation of optimized electroadhesors in a parallel array [7] can exponentially increase the speed at which electronic components are picked and placed on circuit boards and has the potential to revolutionize the electronics manufacturing industry.

5.2. Electroadhesor design blueprint

Having determined the optimal electrode parameters for electroadhesion of millimeter-scale objects, we can now introduce generalized design guidelines.

As mentioned in section 2.1, the optimal parameters can be expressed generally for an electroadhesor of arbitrary size as a ratio of pad area to bounding box area. An optimal pad area to bounding box area ratio of 0.75 was calculated from the optimal pad spacing and pad spacing to pad width ratio. Using this generalized form of the optimal parameters, the electroadhesor can be designed straightforwardly by setting the pad spacing at 0.5 mm and designing pad geometry such that the pad area to bounding box area ratio is 0.75. The pad designs employed in our experiments use a comb-shaped geometry with these parameters; an example implementation of

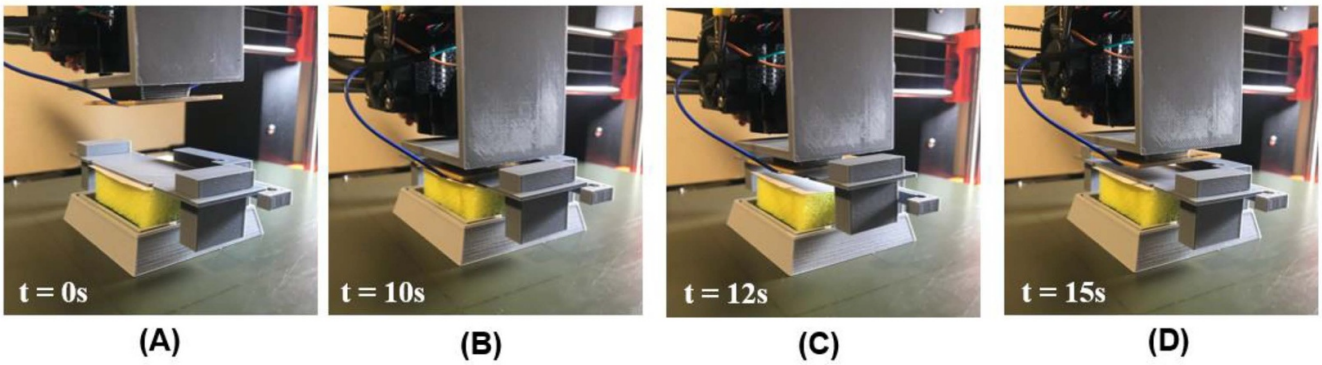


Figure 12. Visual representation of the six-step testing procedure used in the experiment.

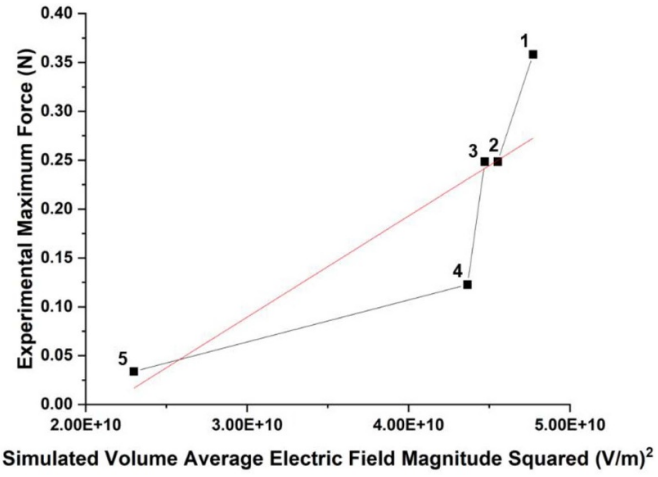


Figure 13. Experimental maximum force as a function of the square of the average electric field magnitude from simulation. The red line is a linear trendline with a 0.834 Pearson correlation coefficient, which is a strong linear trend. Each data point is numbered with the corresponding electroadhesor design number.

this design blueprint using the comb geometry is presented in figure 14.

The comb geometry is only one of infinitely many pad geometries possible using this design blueprint. Since highest electric field magnitude occurs in the area between the two pads, many electroadhesor designs favour highly interdigitated pad geometries as this maximizes electric field magnitude emanating into the object space [6].

5.3. Optimized geometry varies with scale

It should be noted that these optimization results are valid specifically for objects near 1.6 mm thickness. Electric fields emanating from smaller electroadhesor pad spacings decay more quickly in space than those emanating from larger pad spacings [17] as shown in figure 5. As a result, when the thickness of the target object increases, the optimal spacing will also tend to increase as electroadhesors with larger spacings will permeate more of the object space with an electric field, thus creating a greater volume average electric field magnitude and generating a larger force. The same concept applies as object thickness decreases, the optimal spacing will also tend to decrease. Though this relationship is not quantitatively studied extensively in this paper, a systematic study of this relationship between optimal spacing and object thickness will be pursued in future work.

5.4. Two-dielectric electroadhesors

The two-dielectric electroadhesor design allows for significantly higher operating voltages than standard electroadhesors without danger of breakdown. This is a highly effective technique for maximizing electroadhesive force, as it can more than double the average electric field magnitude in the object space. The two-dielectric design is of particular interest for the sub-millimeter pad spacing regime that is the subject of this paper. Since breakdown voltage scales linearly with pad spacing, breakdown voltages become small with decreasing pad spacing. For example, a single dielectric (soldermask) electroadhesor with the optimal spacing of 0.5 mm would have a breakdown voltage of 19.5 kV. Using the two-dielectric design (Teflon for dielectric 1 and neoprene for dielectric 2) with the same electroadhesor geometry, the breakdown voltage would be increased to 35 kV. The increased breakdown voltage is well within the operating range of many commonly used high voltage power supplies, and therefore an increased voltage could reasonably be used for the two-dielectric electroadhesor at this scale. However, the manufacturing of the two-dielectric design presents challenges that are beyond the scope of this work; this was the primary reason the two-dielectric design was not included in our experiments. The problem of manufacturing the two-dielectric design will be approached in future work.

5.5. Sources of error

Electroadhesion is a multivariate phenomenon with over 33 independent factors which are almost impossible to simultaneously control and observe. We believe humidity, and electroadhesor flatness to be the biggest contributors to error.

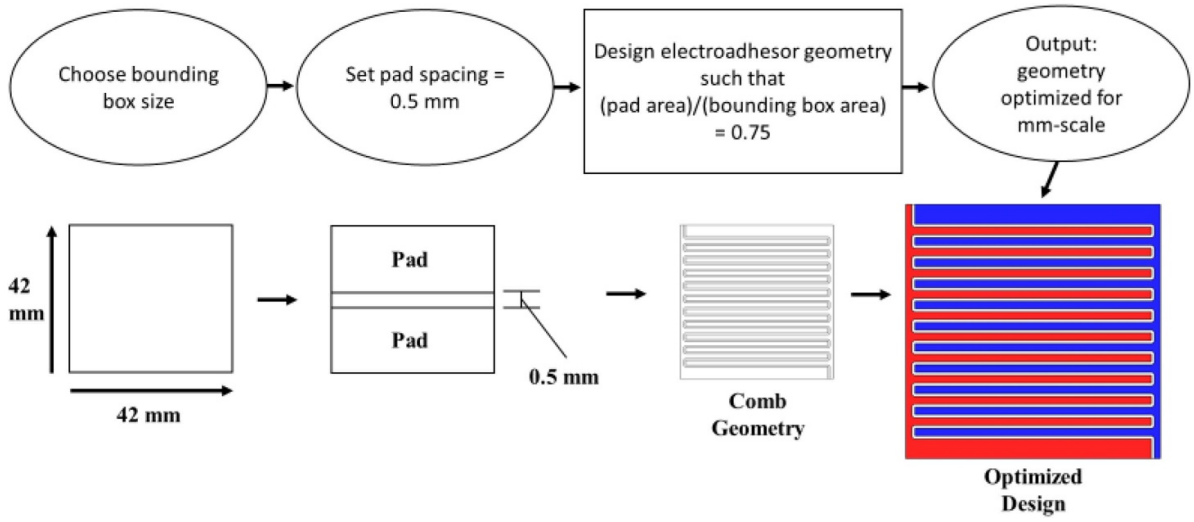


Figure 14. A worked example of the electroadhesor design blueprint using comb geometry.

Final testing was conducted in a two-hour window at 1%–2% fluctuation in humidity to minimize any environmental influence on the experimental results. While the foam desensitized the experiment to angular misalignments between electroadhesor and testing weights, the experiment is still subject to localized flatness changes between testing weights and the face of the electroadhesor.

6. Conclusions and future work

This work introduced a generalized design methodology for optimizing electroadhesors for millimeter-scale objects using sub-millimeter-scale parameters. The methodology was grounded in simulation and experimental data focusing on designs which are both optimal in performance and easily manufacturable. Whenever possible, results were presented in ratios to generalize design rules for electroadhesors of arbitrary bounding box size. The key findings from this study are as follows:

- Optimal pad spacing is achieved in the range of 0.5–0.9 mm for insulative objects. Optimal pad spacing is achieved at 0.5 mm for conductive objects.
- Optimal pad spacing for gripping both insulative and conductive objects is 0.5 mm.
- Optimal pad spacing/pad width for 0.5 mm pad spacing is 0.4.
- Pad spacing, pad width, and pad spacing to pad width ratio can be generalized to the ratio of pad area to bounding box area.
- The optimal pad area to bounding box area for 0.5 mm spacing is 0.75.

These guidelines are particularly relevant for electroadhesive grippers in the electronics industry, wall climbing robots, and astronautical applications.

Electroadhesion is a complex phenomenon which requires further study. Future work may focus on controlling and documenting sources of error such as humidity, barometric pressure, and temperature. Additional efforts will also focus on manufacturing and validating the two-dielectric electroadhesors shown in this study.

Acknowledgments

The authors would like to thank Professor Jeremy Dodd of the Columbia Physics Department and the members of the Creative Machines Laboratory for helping to facilitate and guide this research.

ORCID iD

Jared D West https://orcid.org/0000-0003-3003-0836

References

[1] Guo J, Leng J and Rossiter J 2019 Electroadhesion technologies for robotics: a comprehensive review *IEEE Trans. Robot* **36** 313–27
[2] Monkman G 2003 Electroadhesive microgrippers *Ind. Robot Int. J.* **30** 326–30
[3] Guo J, Tailor M, Bamber T, Chamberlain M, Justham L and Jackson M 2016 Investigation of relationship between interfacial electroadhesive force and surface texture *J. Phys. D: Appl. Phys.* **49** 035303
[4] Monkman G J 1997 An analysis of astrictive prehension *Int. J. Rob. Res.* **16** 1–10
[5] Taylor P M, Monkman G J and Taylor G E 2003 Electrostatic grippers for fabric handling *Proc. IEEE Int. Conf. Robotics and Automation* (https://doi.org/10.1109/ROBOT.1988.12086)
[6] Prahlad H, Pelrine R, Stanford S, Marlow J and Kornbluh R 2008 Electroadhesive robots—wall climbing robots enabled by a novel, robust, and electrically controllable adhesion technology *Proc. IEEE Int. Conf. Robotics and Automation*
[7] Mici J, Ko J W, West J and Lipson H 2019 Parallel electrostatic grippers for layered assembly *J. Addit. Manuf.* **27** 451–60

[8] Leung B C, Goeser N R, Miller L A and Gonzalez S 2015 Validation of electroadhesion as a docking method for spacecraft and satellite servicing *IEEE Aerospace Conf. Proc.* pp 1–8
[9] Ritter M and Barnhart D 2017 Geometry characterization of electroadhesion samples for spacecraft docking application *IEEE Aerospace Conf. Proc.* (https://doi.org/10.1109/AERO.2017.7943683)
[10] Kim S *et al* 2019 Soft nanocomposite electroadhesives for digital micro- and nanotransfer printing *Sci. Adv.* **5** 10
[11] Ruffatto D, Shah J and Spenko M 2013 Optimization and experimental validation of electrostatic adhesive geometry *IEEE Aerospace Conf. Proc.* (https://doi.org/10.1109/AERO.2013.6496943)
[12] Guo J, Bamber T, Chamberlain M, Justham L and Jackson M 2016 Optimization and experimental verification of coplanar interdigital electroadhesives *J. Phys. D: Appl. Phys.* **49** 415304
[13] Sogard M R, Mikkelson A R, Nataraju M, Turner K T and Engelstad R L 2007 Analysis of Coulomb and Johnsen–Rahbek electrostatic chuck performance for EUV lithography *Comput. Mech.* **2** 1–30
[14] Griffiths D 1999 *Introduction to Electrodynamics* (Upper Saddle River, NJ: Prentice Hall)
[15] Ruffatto D, Shah J and Spenko M 2014 Increasing the adhesion force of electrostatic adhesives using optimized electrode geometry and a novel manufacturing process *J. Electrostat.* **72** 147–55
[16] Guo J, Bamber T, Hovell T, Chamberlain M, Justham L and Jackson M 2016 Geometric optimisation of electroadhesive actuators based on 3D electrostatic simulation and its experimental verification *IFAC* **49** 309–15
[17] Ruffatto D, Shah J and Spenko M 2012 Optimization of electrostatic adhesives for robotic climbing and manipulation *Proc. ASME Design Engineering Technical Conf.*
[18] Monkman G J 2007 *Robot Grippers* (Weinheim: Wiley)
[19] Anon 2019 *LPKF S64 Data Sheet*
[20] Li Q, Rudolph V and Peukert W 2006 London-van der Waals adhesiveness of rough particles *Powder Technol.* **161** 248–55
[21] Huber E, Mirzaee M, Bjorgaard J, Hoyack M, Noghanian S and Chang I 2016 Dielectric property measurement of PLA *IEEE Int. Conf. Electro. Inf. Technol*. pp 788–92